Ultrabroadband spin-wave propagation in $Co_2(Mn_{0.6}Fe_{0.4})Si$ thin films

Tobias Stückler,[1] Chuanpu Liu,[1,2] Tao Liu,[3] Haiming Yu,[1,*] Florian Heimbach,[1] Jilei Chen,[1] Junfeng Hu,[1] Sa Tu,[1] Youguang Zhang,[1] Simon Granville,[4,†] Mingzhong Wu,[3] Zhi-Min Liao,[2] Dapeng Yu,[2,5] and Weisheng Zhao[1]

[1]*Fert Beijing Research Institute, School of Electrical and Information Engineering, BDBC, Beihang University, Beijing 100191, People's Republic of China*

[2]*State Key Laboratory for Mesoscopic Physics, School of Physics, Peking University, Beijing 100871, People's Republic of China*

[3]*Department of Physics, Colorado State University, Fort Collins, Colorado 80523, USA*

[4]*MacDiarmid Institute for Advanced Materials and Nanotechnology, Robinson Research Institute, Victoria University of Wellington, P.O. Box 33436, Lower Hutt 5046, New Zealand*

[5]*Physics Department, Southern University of Science and Technology, Shenzhen 518055, People's Republic of China*

(Received 28 April 2017; revised manuscript received 18 July 2017; published 25 October 2017)

Ferromagnetic Heusler alloys with low magnetic damping are highly promising materials for magnonic devices, which rely on the excitation and detection of spin waves. Using all-electrical spin-wave spectroscopy we report spin-wave propagation in sputtered $Co_2(Mn_{0.6}Fe_{0.4})Si$ Heusler alloy thin films with a thickness of 50 nm. We integrated a nanostructured microwave antenna to locally excite and detect propagating spin waves in a Damon-Eshbach configuration. We estimate the group velocity to be up to 12.0 km/s and we observe spin-wave propagation with a frequency band as broad as 15 GHz. From the experimental frequency dependence of group velocity we calculate the spin-wave dispersion. Our results show that all-electrical measurements are a powerful method for determining the fundamental spin-wave characteristics of Heusler alloys, over a broad and tunable range of frequencies, and with group velocities an order of magnitude higher than in conventional materials.

DOI: 10.1103/PhysRevB.96.144430

I. INTRODUCTION

For a long time the ferrimagnetic insulator $Y_3Fe_5O_{12}$ (YIG) has been one of the most promising materials for spin-wave applications, due to its very small saturation magnetization, a small damping parameter 10^{-5} [1], and its large spin-wave decay length of over 500 μm [2]. A problem of YIG is that it is almost exclusively grown on $Gd_3Ga_5O_{12}$ (GGG) substrates, which are incompatible with complementary metal oxide semiconductor (CMOS) technology. In addition, the group velocity of YIG is small at around 1 km/s. So other materials such as CoFeB and permalloy ($Ni_{80}Fe_{20}$), which are utilized in magnetic tunnel junctions (MTJs) to build magnetic random access memories (MRAMs), or read heads and spin-logic devices [3–5], are considered as interesting alternatives. However, these ferromagnetic metals have higher damping and smaller propagation distances than YIG. Another promising class of materials for magnonics are full Heusler alloys with the formula X_2YZ, where X and Y are transition or rare-earth metals and the element Z is a main group element [6]. Some of these are half metals, with a theoretically predicted spin polarization of 100%, making them very interesting for spintronic applications [7,8], and they have already been proven to be compatible with many spintronic devices [9,10]. It is possible to grow them with a low damping of around 10^{-3} [11] or even lower [12], and half-metallic Heuslers also show high group velocities up to 26 km/s [13], which makes them interesting for magnonics. Some spin-wave propagation work has already been reported on Heusler alloys using Brillouin light scattering [11], but there is a lack of all-electrical measurements on such materials.

II. METHODS

In this paper we report a study of spin-wave propagation in the Heusler alloy $Co_2(Mn_{0.6}Fe_{0.4})Si$ (CMFS) and determine the damping and group velocity of the material, as well as the nonreciprocity effect of the experimental system. All measurements have been performed at room temperature (300 K). After sputtering a 5 nm layer of MgO on a Si(100) substrate at room temperature, CMFS films of around 50 nm thickness have been sputtered at 450 °C, followed by a capping layer of 5 nm MgO deposited at room temperature to protect the surface. For our measurements, we used two identical films. One has been left unpatterned for superconduction quantum interference device (SQUID), x-ray diffraction (XRD), and ferromagnetic resonance (FMR) measurements, and the other one has been patterned into strips with a size of 300 × 16 μm using optical lithography and ion beam etching. After the etching, the strips have been covered with a 15-nm-thick sputtered film of Al_2O_3 used as an insulating layer to avoid electrical contact with the antennas, which have been produced in the next step. The antennas were prepared by electron beam lithography, sputtering, and a lift-off process. They consist of gold and have a thickness of 120 nm.

III. MEASUREMENT RESULTS

We first talk about our measurements on the plain film. XRD shows the presence of (220) reflection of the cubic Heusler structure corresponding to a lattice parameter of 5.65 Å. In Fig. 1(a) we see a magnetization measurement performed on the unpatterned film at 300 K. The coercive field is $\Delta\mu_0 H_c = 1.5$ mT, the material is saturated above $\Delta\mu_0 H_S = 10$ mT, and the saturation magnetization is 812 emu/cc, 3.95μ_B per formula unit, or 1.02 T/μ_0.

The FMR measurements were performed by a shorted K_u-band rectangular waveguide with field modulation and

*haiming.yu@buaa.edu.cn
†simon.granville@vuw.ac.nz

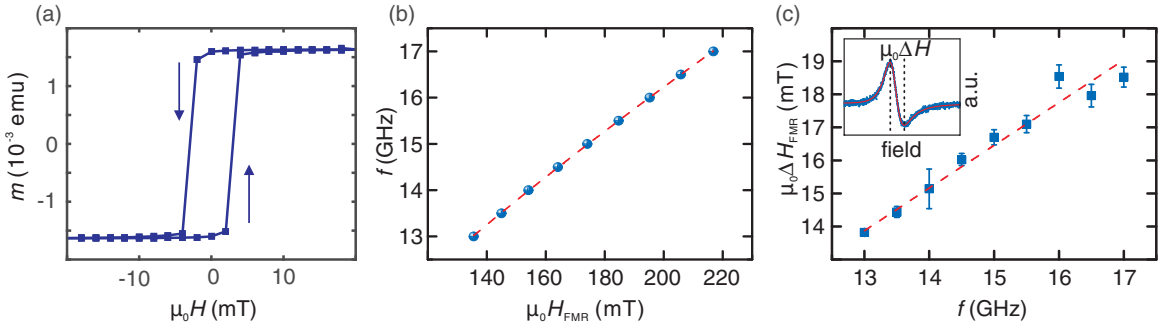

FIG. 1. (a) SQUID magnetization measurement at 300 K of the unpatterned film. (b) Resonance frequency over resonance field and (c) FMR linewidth $\mu_0\Delta H_{\mathrm{FMR}}$ plotted over the resonance frequency for the FMR data. The inset shows a typical resonance curve for a frequency of 13 GHz, which is used to obtain the FMR linewidth $\mu_0\Delta H_{\mathrm{FMR}}$ from the Lorentzian fitting (red) of the experimental data (blue).

lock-in detection techniques. FMR data have been measured for different frequencies. The inset of Fig. 1(c) shows a typical FMR measurement at a frequency of 13 GHz. The blue dots mark the experimental data and the red curve represents a Lorentzian fitting which is used to obtain the resonance field $\mu_0 H_{\mathrm{FMR}}$ and the FMR linewidth $\mu_0\Delta H_{\mathrm{FMR}}$. In Fig. 1(b) we plot $\mu_0 H_{\mathrm{FMR}}$ (blue) over f and fit to the Kittel formula (red),

$$f = |\gamma|\sqrt{\mu_0 H_{\mathrm{FMR}}(\mu_0 H_{\mathrm{FMR}} + M_{\mathrm{S}})}, \tag{1}$$

to obtain the gyromagnetic ratio γ and the saturation magnetization M_{S}. In Fig. 1(c) we plot $\mu_0\Delta H_{\mathrm{FMR}}$ over f (blue) and fit it linearly (red) to

$$\mu_0\Delta H_{\mathrm{FMR}} = \frac{2\alpha f}{\sqrt{3}|\gamma|} + \mu_0\Delta H_0, \tag{2}$$

with the damping α. A more detailed explanation of the analysis technique can be found in Chang *et al.* [1]. The fitting yields the parameters $\alpha = (1.04 \pm 0.06) \times 10^{-2}$, $|\gamma| = (32.2 \pm 4.3)$ GHz/T, $\mu_0\Delta H_0 = 8.03 \pm 5.0$ mT, and $\mu_0 M_{\mathrm{S}} = 1.07 \pm 0.03$ T, which is in good agreement with the SQUID measurements. The structure and magnetization values obtained are fairly typical for sputtered $Co_2(Mn_{0.6}Fe_{0.4})Si$ films [14,15].

Now we show results of the patterned films. In Fig. 2(b) we see a scanning electron microscopy (SEM) picture of these so-called nanostripline (NSL) antennas. Their width was determined to be around 128 nm and the distance between the two NSLs is 2 μm. For the spin-wave propagation measurements, we applied an external in-plane magnetic field parallel to the antennas, using a vector network analyzer (VNA) to induce an rf current into the antenna. Figure 2(a) shows the schematic of the device. The VNA applied the current for different frequencies and detected the scattering parameter [16]. The dynamic magnetic field of the induced rf current excited a spin wave with a k vector perpendicular to the magnetic field. These are so-called Damon-Eshbach (DE) type spin waves. For these measurements, we used the sample with two NSL antennas. One antenna acts as a spin-wave emitter and the other one as a detector [17]. In Fig. 2(c) we show the imaginary part of the transmission signal S_{12} from a measurement with the integrated NSL antenna. The external magnetic field was swept from -100 to $+100$ mT in steps of 0.5 mT. For every field the rf current was swept from 10 MHz to 20 GHz. We observe one strong ultrabroad mode over the whole field range. In Fig. 2(d) we see a cut of the full spectrum at $\mu_0 H = -10$ mT with very clear oscillations. Our measurement technique excites spin waves with different wave vectors k, which we will explain later. Because of the different wave vectors k we have spin waves with different wavelengths, resulting in the measured frequency band, for one specific external field. As the distance between our antennas is fixed, different wavelengths show a phase change in the detected signal, so that these amplitude oscillations prove spin-wave propagation between the two NSLs. The frequency separation Δf between two neighboring minima represents a phase change of 2π [18,19] and can be used to calculate the group velocity by

$$v_{\mathrm{g}} = \frac{\delta\omega}{\delta k} \approx \frac{2\pi\Delta f}{2\pi/s} = \Delta f \times s, \tag{3}$$

where $s = 2$ μm is the distance between the two NSLs.

By comparing the signal for negative and positive external fields in Fig. 2(c) we see a clear discrepancy. For negative

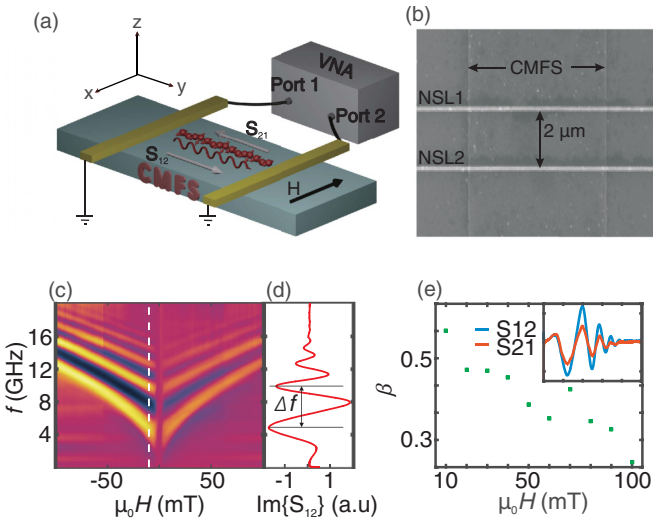

FIG. 2. (a) Schematic of the studied device using VNA and NSL antennas (yellow) prepared on CMFS (gray) with spin-wave propagation (red) in two directions S_{12} and S_{21}. (b) SEM picture of a CMFS mesa with two NSL antennas. The distance between the antennas is 2 μm and the width is around 128 nm. (c) Color coded spectra of spin-wave propagation data S_{12} as a function of $\mu_0 H$. The line spectrum in (d) is a cut of the full spectrum shown by the white dotted line at $\mu_0 H = -10$ mT. (e) Nonreciprocity parameter β of the experimental setup.

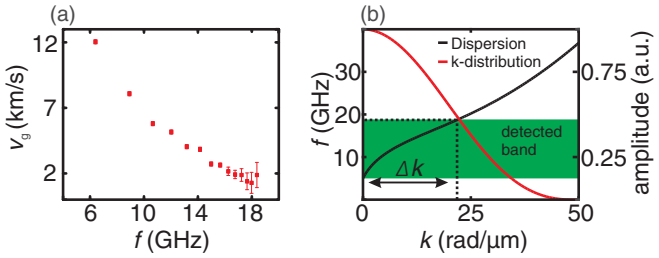

FIG. 3. (a) Group velocity for different frequencies at $\mu_0 H = -10$ mT, and (b) calculated dispersion relation (black) of the device and k excitation (red) of the NSL. The green area shows the detected frequency band in the measurement.

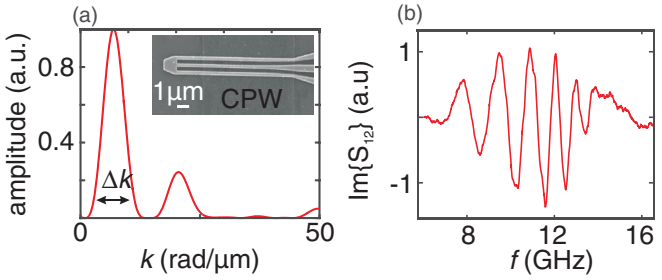

FIG. 4. (a) k distribution of the CPW and (b) a cut of the full spectrum at -10 mT.

fields the signal is much stronger than for positive fields. This can be explained by the nonreciprocity effect. In Fig. 2(e) the nonreciprocity parameter, which is defined as $\beta = S_{12}/S_{21}$, is shown over the external magnetic field. The inset compares the signal S_{12} and S_{21} at the external field $\mu_0 H = -10$ mT, which is equivalent to comparing the signal of only S_{12} or S_{21} at external fields $\mu_0 H = \pm 10$ mT. If the spin-wave propagation were completely symmetric for propagation from the first to the second NSL and vice versa with the same external field direction, β would be 1. We see for our measurement strong differences with β between 0.3 and 0.6.

The two dominant effects leading to nonreciprocity in our system are, on one hand, the intrinsic nonreciprocal character, which can be observed for DE surface modes [20], and, on the other hand, the specific excitation effect of the antennas [21,22]. The specific excitation effect is sensitive to the direction of the spin-wave propagation, which can be parallel or antiparallel to the rf magnetic field. The nonreciprocity related to the excitation of the antenna becomes larger for a smaller antenna width, because the excitation effect at the edges of the antenna becomes more substantial. With a width of 128 nm and a thickness of 120 nm, our antennas have a nearly square cross section, so the y and the z components of the dynamic field become almost equivalent [23]. Our observed nonreciprocity is higher compared to other works [21]. A high nonreciprocity is an important characteristic for nonreciprocity-based magnonic devices [24].

In Fig. 3(a) we see the change of the group velocity v_g at $\mu_0 H = -10$ mT for different frequencies. We define the frequency point f as the middle between two neighboring extrema of the oscillation. With this separation $\Delta f/2$ we calculate the group velocity for different frequencies. We find a group velocity of around 12.0 km/s for the lowest frequency. The velocity does level off above ~16 GHz with a lowest point at almost 1.3 km/s for approximately 18 GHz. Starting with the form of the dispersion relation according to Stancil and Prabhakar [25], the saturation magnetization $\mu_0 M_S = 1.02$ T from the SQUID measurement, and the anisotropy field $\mu_0 H_{ani}$, we can derive the dependence of the group velocity on the frequency. We find $\mu_0 H_{ani} = 0.02$ T allows us to reproduce the experimental group velocity data of Fig. 3(a), and the corresponding dispersion relation is shown in Fig. 3(b). Also shown is the calculated k excitation of the NSL. As predicted from Ciubotaru *et al.* [17] and Kennewell *et al.* [26], the NSL excites a very broad Δk for spin waves, with the main peak at $k = 0$. According to the dispersion relation, we have a very broad frequency band starting at around 5 GHz and theoretically going up to very high frequencies of over 30 GHz. Due to the decreasing excitation amplitude with increasing frequency, our detected frequency band (green) is limited to around 18 GHz.

To further investigate spin-wave propagation we also used the technique of coplanar waveguides (CPWs) to excite spin waves. A CPW has a specific excitation for $k \neq 0$ [2], so it is interesting to study and compare both techniques on the same material. The signal line of our CPW has a width of 180 nm and the ground lines have a width of 200 nm. They consist of gold and have a thickness of 120 nm. The calculated k excitation of the CPW is shown in Fig. 4(a). By contrast with the NSL excitation, the main excitation for the CPW is at $k \neq 0$, with smaller Δk. This results in an upshift of the resonance mode for the CPW measurement [Fig. 4(b)]. There we see a cut of the full spectrum of the CPW measurement at -10 mT. If we compare this to the line spectrum of the NSL [Fig. 2(d)], we see that the oscillations start at higher frequencies of around 7 GHz. The excitation band for the CPW from around 7 to 16 GHz is still very broad, but it is narrower than the band for the NSL measurement. This is the result of the smaller Δk excitation in the CPW measurement. In similar works, normally CPWs with a thicker signal line of around 2 μm are used [2,27], which show narrower Δk excitation. So the dimensions of an antenna can be used to tune the limit of the excitation band and a CPW can be used to excite specific wave vectors with $k \neq 0$. This could be an interesting development, allowing the simultaneous generation of spin waves with different wave vectors, which can be superposed for magnonic logic operations [28–30].

IV. DISCUSSION

Finally, we discuss the key factors that highlight the great promise of sputtered thin films of CMFS and other Heusler alloys for high-performance magnonic devices—the group velocity and damping constant.

The maximal group velocity is several times higher than previously reported for CMFS [31]. Regarding Eq. (3), we see that the group velocity is the derivative of the dispersion relation. The main material parameter influencing the slope of the dispersion relation [25] is the saturation magnetization. Our determined saturation magnetization is fairly typical for sputtered CMFS films [14,32] and one order higher than YIG, for example [2]. Compared to conventional magnetic

thin films, the maximum group velocity in the CMFS film of 12.0 km/s is smaller than the maximum achieved in the highest-quality films of CoFeB, but it is an order of magnitude higher than in thin-film YIG, the best material for pure spin-wave propagation [2,31,33]. In addition, experimentally determined spin-wave dispersion relations for half-metallic Heusler alloys are scarce in the literature [34,35], and results such as Fig. 3(b) will allow spin-wave calculations to be refined and will help determine the usefulness of such materials for magnonic devices.

For spin waves that can be detected over long enough distances to be used in microelectronics, the damping constant α needs to be kept to a minimum. The damping constant of our films is ∼0.01, in agreement with previous studies of CMFS films produced by magnetron sputtering [14]. However, in those studies it has also been shown that the damping of CMFS and related Heusler alloys depends very sensitively on the film composition and annealing conditions [14,36]. Damping values of 0.003 have been achieved in the highest-quality Heusler thin films deposited by molecular beam epitaxy on single-crystalline MgO substrates [13], and, very recently, using an underlayer of Cr resulted in sputtered CMFS films with damping values around 0.0045 [37]. These results show that it should be possible to optimize the damping properties of CMFS grown by magnetron sputtering, resulting in an increased spin-wave propagation length.

V. CONCLUSION

In conclusion, the coercive field, the saturation field, the damping, the gyromagnetic ratio, and the saturation magnetization of the Heusler alloy $Co_2(Mn_{0.6}Fe_{0.4})Si$ have been determined from measurements on an unpatterned sample, which we use to calculate the dispersion relation for the measurement with the patterned film. On this patterned film, we have performed spin-wave propagation measurements, detected from oscillations in the imaginary part of the spectra. For NSL antennas, we observed spin-wave propagation over an ultrabroad frequency band over 15 GHz. We detect this ultrabroad frequency band in one measurement without needing to change or adjust the experimental setup. We detect group velocities up to an order of magnitude greater than in YIG, varying in the band from 12.0 km/s at low frequency to 1.3 km/s at higher frequencies. Furthermore, we characterized the strong nonreciprocity effect of the NSL antennas and compared the technique with CPW excitation. The NSL measurement shows a much broader frequency band excitation from the higher Δk, while the dimensions of a CPW can be more easily used to limit the frequency band. The flexibility of these all-electrical excitation schemes could be an advantage for magnonic applications, particularly with a promising materials class such as the ferromagnetic Heusler alloys.

ACKNOWLEDGMENTS

We wish to acknowledge support from the National Nature Science Foundation of China under Grants No. 11674020 and No. 11444005, Youth 1000 Talent Program, 111 Talent Program B16001, and Ministry of Science and Technology of China MOST No. 2016YFA0300802. The work at CSU was supported by SHINES, an Energy Frontier Research Center funded by the US Department of Energy (SC0012670), and the US National Science Foundation (EFMA-1641989). We gratefully acknowledge equipment support from the MacDiarmid Institute.

T.S. and C.L. contributed equally to this work.

[1] H. Chang, P. Li, W. Zhang, T. Liu, A. Hoffmann, L. Deng, and M. Wu, IEEE Magn. Lett. **5**, 1 (2014).
[2] H. Yu, O. d. A. Kelly, V. Cros, R. Bernard, P. Bortolotti, A. Anane, F. Brandl, R. Huber, I. Stasinopoulos, and D. Grundler, Sci. Rep. **4**, 6848 (2014).
[3] J. S. Moodera, L. R. Kinder, T. M. Wong, and R. Meservey, Phys. Rev. Lett. **74**, 3273 (1995).
[4] S. Parkin, C. Kaiser, A. Panchula, P. M. Rice, B. Hughes, M. Samant, and S. H. Yang, Nat. Mater. **3**, 862 (2004).
[5] S. Ikeda, K. Miura, H. Yamamoto, K. Mizunuma, H. D. Gan, M. Endo, S. L. Kanai, J. Hayakawa, F. Matsukura, and H. Ohno, Nat. Mater. **9**, 721 (2010).
[6] C. Felser and B. Hillebrands, J. Phys. D **42**, 080301 (2009).
[7] M. I. Katsnelson, V. Y. Irkhin, L. Chioncel, A. I. Lichtenstein, and R. A. De Groot, Rev. Mod. Phys. **80**, 315 (2008).
[8] H. C. Kandpal, G. H. Fecher, C. Felser, and G. Schönhense, Phys. Rev. B **73**, 094422 (2006).
[9] G. Ortiz, A. Garcia, J. B. Youssef, N. Biziere, F. Boust, J. F. Bobo, E. Snoeck, and N. Vukadinovic, IEEE Trans. Magn. **49**, 1037 (2013).
[10] Z. Bai, L. Shen, G. Han, and Y. P. Feng, SPIN **02**, 1230006 (2012).
[11] T. Sebastian, Y. Ohdaira, T. Kubota, P. Pirro, T. Brächer, K. Vogt, A. A. Serga, H. Naganuma, M. Oogane, Y. Ando, and B. Hillebrands, Appl. Phys. Lett. **100**, 112402 (2012).
[12] S.-Z. Qiao, Q.-N. Ren, R.-R. Hao, H. Zhong, Y. Kang, S.-S. Kang, Y.-F. Qin, S. Y. Yu, G.-B. Han, S.-S. Yan, and L.-M. Mei, Chin. Phys. Lett. **33**, 047601 (2016).
[13] L. M. Loong, J. H. Kwon, P. Deorani, C. N. T. Yu, A. Hirohata, and H. Yang, Appl. Phys. Lett. **104**, 232409 (2014).
[14] T. Kubota, S. Tsunegi, M. Oogane, S. Mizukami, T. Miyazaki, H. Naganuma, and Y. Ando, Appl. Phys. Lett. **94**, 122504 (2009).
[15] Y. Sakuraba, M. Ueda, Y. Miura, K. Sato, S. Bosu, K. Saito, M. Shirai, T. J. Konno, and K. Takanashi, Appl. Phys. Lett. **101**, 252408 (2012).
[16] S. Neusser, Ph.D. thesis, Universität München, 2011.
[17] F. Ciubotaru, T. Devolder, M. Manfrini, C. Adelmann, and I. P. Radu, Appl. Phys. Lett. **109**, 012403 (2016).
[18] S. Neusser, G. Dürr, H. G. Bauer, S. Tacchi, M. Madami, G. Woltersdorf, G. Gubbiotti, C. H. Back, and D. Grundler, Phys. Rev. Lett. **105**, 067208 (2010).
[19] V. Vlaminck and M. Bailleul, Science **322**, 410 (2008).
[20] A. A. Serga, A. V. Chumak, and B. Hillebrands, J. Phys. D **43**, 264002 (2010).
[21] K. Sekiguchi, K. Yamada, S. M. Seo, K. J. Lee, D. Chiba, K. Kobayashi, and T. Ono, Appl. Phys. Lett. **97**, 022508 (2010).
[22] V. E. Demidov, M. P. Kostylev, K. Rott, P. Krzysteczko, G. Reiss, and S. O. Demokritov, Appl. Phys. Lett. **95**, 112509 (2009).
[23] P. Deorani, J. H. Kwon, and H. Yang, Curr. Appl. Phys. **14**, S129 (2014).

[24] M. Jamali, J. H. Kwon, S.-M. Seo, K.-J. Lee, and H. Yang, Sci. Rep. **3**, 3160 (2013).
[25] D. D. Stancil and A. Prabhakar, *Spin Waves* (Springer, Berlin, 2009).
[26] K. J. Kennewell, M. Kostylev, and R. L. Stamps, J. Appl. Phys. **101**, 09D107 (2007).
[27] J. Chen, F. Heimbach, T. Liu, H. Yu, C. Liu, H. Chang, T. Stückler, J. Hu, L. Zeng, Y. Zhang *et al.*, J. Magn. Magn. Mater., doi:10.1016/j.jmmm.2017.04.045 (2017).
[28] B. Lenk, H. Ulrichs, F. Garbs, and M. Münzenberg, Phys. Rep. **507**, 107 (2011).
[29] T. Fischer, M. Kewenig, D. A. Bozhko, A. A. Serga, I. I. Syvorotka, F. Ciubotaru, C. Adelmann, B. Hillebrands, and A. V. Chumak, Appl. Phys. Lett. **110**, 152401 (2017).
[30] K. Vogt, F. Y. Fradin, J. E. Pearson, T. Sebastian, S. D. Bader, B. Hillebrands, A. Hoffmann, and H. Schultheiss, Nat. Commun. **5**, 3727 (2014).
[31] A. V. Chumak, A. A. Serga, and B. Hillebrands, J. Phys. D **50**, 244001 (2017).
[32] M. Oogane, T. Kubota, N. Hirose, and Y. Ando, J. Magn. Soc. Jpn. **33**, 270 (2009).
[33] H. Yu, R. Huber, T. Schwarze, F. Brandl, T. Rapp, P. Berberich, G. Duerr, and D. Grundler, Appl. Phys. Lett. **100**, 262412 (2012).
[34] J. Thoene, S. Chadov, G. Fecher, C. Felser, and J. Kübler, J. Phys. D **42**, 084013 (2009).
[35] J. Chico, S. Keshavarz, Y. Kvashnin, M. Pereiro, I. Di Marco, C. Etz, O. Eriksson, A. Bergman, and L. Bergqvist, Phys. Rev. B **93**, 214439 (2016).
[36] M. Oogane, T. Kubota, H. Naganuma, and Y. Ando, J. Phys. D **48**, 164012 (2015).
[37] S. Pan, T. Seki, K. Takanashi, and A. Barman, Phys. Rev. Appl. **7**, 064012 (2017).